7444–7459 *Nucleic Acids Research, 2019, Vol. 47, No. 14* *Published online 31 May 2019*
doi: 10.1093/nar/gkz473

A *Drosophila* cell-free system that senses DNA breaks and triggers phosphorylation signalling

Lisa Harpprecht[1], Sandro Baldi[1,2], Tamas Schauer[1,3], Andreas Schmidt[1,4], Tanja Bange[5], Maria S. Robles[5], Elisabeth Kremmer[6], Axel Imhof[1,2,4] and Peter B. Becker[1,2,*]

[1]Molecular Biology Division, Biomedical Center, LMU Munich, 82152 Planegg-Martinsried, Germany, [2]Center for Integrated Protein Science Munich, LMU Munich, 81377 Munich, Germany, [3]Bioinformatics Unit, Biomedical Center, LMU Munich, 82152 Planegg-Martinsried, Germany, [4]Protein Analysis Unit, Biomedical Center, LMU Munich, 82152 Planegg-Martinsried, Germany, [5]Institute of Medical Psychology, LMU Munich, 80336 Munich, Germany and [6]Institute of Molecular Immunology, German Research Center for Environmental Health, 81377 Munich, Germany

Received March 22, 2019; Revised May 13, 2019; Editorial Decision May 15, 2019; Accepted May 16, 2019

ABSTRACT

Preblastoderm *Drosophila* embryo development is characterized by fast cycles of nuclear divisions. Extracts from these embryos can be used to reconstitute complex chromatin with high efficiency. We now discovered that this chromatin assembly system contains activities that recognize unprotected DNA ends and signal DNA damage through phosphorylation. DNA ends are initially bound by Ku and MRN complexes. Within minutes, the phosphorylation of H2A.V (homologous to γH2A.X) initiates from DNA breaks and spreads over tens of thousands DNA base pairs. The γH2A.V phosphorylation remains tightly associated with the damaged DNA and does not spread to undamaged DNA in the same reaction. This first observation of long-range γH2A.X spreading along damaged chromatin in an *in vitro* system provides a unique opportunity for mechanistic dissection. Upon further incubation, DNA ends are rendered single-stranded and bound by the RPA complex. Phosphoproteome analyses reveal damage-dependent phosphorylation of numerous DNA-end-associated proteins including Ku70, RPA2, CHRAC16, the exonuclease Rrp1 and the telomer capping complex. Phosphorylation of spindle assembly checkpoint components and of microtubule-associated proteins required for centrosome integrity suggests this cell-free system recapitulates processes involved in the regulated elimination of fatally damaged syncytial nuclei.

INTRODUCTION

DNA damage in higher eukaryotes must be viewed as chromatin damage. After all, the chromatin organization of complex genomes affects all aspects of the DNA damage response: the recognition of the lesion in the nucleosome fibre, the signalling to coordinate the repair machinery with cell cycle regulators and the repair process itself. The complexity of the chromatin damage response is reflected by the involvement of a large number of structural proteins and enzymes that 'remodel' chromatin before, during and after the actual DNA repair [for reviews, see (1–5)].

Cell-free systems can be used to mechanistically understand the processes revolving around damaged chromatin. The two most prominent experimental systems for the reconstitution of chromatin with physiological properties are derived from *Xenopus laevis* eggs or oocytes (6), and preblastoderm embryos of *Drosophila melanogaster* (7,8). In both models, the fertilized eggs contain large stockpiles of maternal proteins and RNA that support the first 12 cell divisions, or 13 nuclei divisions, respectively, in the absence of significant transcription (9).

We pioneered extracts of preblastoderm *Drosophila* embryos (on average 1.5 h old) to assemble dynamic, complex chromatin with physiological properties with very high efficiency (7,8). The extract is a rich source of ATP-dependent nucleosome remodelling factors. Indeed, the ISWI-containing nucleosome sliding factors NURF, CHRAC and ACF have been first identified and isolated from this extract (10–12). We recently reconstituted chromatin genome-wide and discovered faithful nucleosome phasing at prominent sites (13).

We now discovered that chromatin reconstitution on linear DNA (featuring unprotected ends) leads to phosphorylation of H2A.V at its C-terminus. H2A.V, the only H2A variant in flies, resembles the orthologous H2A.Z in yeast and mammals, but in addition bears the C-

*To whom correspondence should be addressed. Tel: +49 89 2180 75427; Fax: +49 89 2180 75425; Email: pbecker@bmc.med.lmu.de

terminal SQAY sequence that serves as acceptor for DNA damage-associated phosphorylation by ATM and ATR [reviewed in (14–16)]. In response to DNA double-strand breaks (DSBs), phosphorylation of H2A.V at S137 leads to γH2A.V, in direct analogy to γH2A.X (17,18). The observed γH2A.V signal suggests that the chromatin reconstitution system senses free DNA ends and mounts some type of signalling response.

The first 13 syncytial nuclear replication cycles in *Drosophila* embryos are extremely fast. Since they lack the G phases of the cell cycle when there is no time to repair DSBs (19). In these stages, nuclei signal the presence of broken chromosomes not to halt the cell cycle for repair, but rather to induce their elimination (20). The fly orthologues of mammalian ATM and ATR kinases are active in cleavage-stage embryos and involved in DSB signalling (18). The downstream checkpoint kinase dChk1 is kept inactive until cycle 13/14, when it's activity orchestrates the first cell cycle arrest to give time for the 'mid-blastula transition (MBT) (21). By contrast, Chk2 is active early on and is involved in DSB signalling that eventually leads to centrosome inactivation, the disruption of the mitotic spindles and defects in chromosome segregation, so that the affected nuclei are not localized to the embryo cortex, but rather 'drop out' to the interior of the syncytium, where they are degraded (20).

We now present an initial characterization of the response of the *Drosophila* embryo extract to DNA breaks. We systematically describe the chromatin association of repair-related protein factors and dynamic changes of the phosphoproteome in reconstituted chromatin and in response to DNA ends. We observe an initial binding of several DNA end-binding complexes known for their role in damage signalling and document a wave of phosphorylation triggered by DSB. We furthermore identified phosphorylation targets in response to DSBs pointing towards an active preblastoderm embryo damage response in our system. Remarkably, we also observe a very fast spreading of the γH2A.V phosphorylation signal from a DNA break over tens of thousands base pairs along the folded nucleosome fibre. *In vivo*, the γH2A.X signal 'spreads' from a DNA break over hundreds of kilobases in yeast (22) and thousands of kilobases in mammals (23) to establish a DNA damage domain. The cell-free reconstitution system provides a useful tool for further mechanistic dissection of this spreading process and of other aspects of the dsDNA break response in cleavage stage embryos. It allowed us to analyse the recruitment of damage-associated complexes to DSBs at early and late time points, to investigate the development of H2A.V phosphorylation along DSBs shortly after damage recognition, and to obtain a list of phosphorylation targets in response to DSBs.

MATERIALS AND METHODS

Preparation of *Drosophila* preblastoderm embryo extract

Drosophila embryo extract was prepared from preblastoderm embryos within 90 min after egg laying as described (7), with modifications. The embryos were dechorionated in 200 ml embryo wash buffer (EW: 0.7% NaCl, 0.04% Triton X-100) and 60 ml 13% sodium hypochlorite (VWR) for 3 min at room temperature (RT) while stirring. Embryos were rinsed for 5 min with cold water and transferred into a glass cylinder with EW. Settled embryos were washed first in 0.7% NaCl and then in extract buffer (10 mM HEPES, pH 7.6, 10 mM KCI, 1.5 mM $MgCl_2$, 0.5 mM EGTA, 10% glycerol, 10 mM 3-glycerophosphate; 1 mM DTT, protease inhibitors added freshly before use (0.2 mM PMSF, 1 mM Aprotinin, 1 mM Leupeptin, 1 mM Pepstatin). Embryos were settled in a homgen^{plus} homogenizer (Schuett-Biotec), the supernatant was decanted and homogenized with one stroke at 3000 rpm and 10 strokes at 1500 rpm. The $MgCl_2$ concentration of the homogenate was adjusted to 5 mM (f.c.) and centrifuged for 15 min at 27 000 *g* at 4°C. The white lipid layer was discarded and the supernatant was centrifuged for 2 h at 245 000 *g* at 4°C. The clear extract was collected with a syringe, leaving the lipid layer and pellet behind.

Immobilization of DNA

Short plasmids (pUC18) or long fosmids (fosmids 019611 and 019829, (24) were used as closed circles or linearized with XbaI in case of pUC18, or FseI, RsrII, in case of fosmid 019611 or SgrDI in case of fosmid 019829, respectively. For some assays, DNA was bound to streptavidin-coated paramagnetic beads (25). For immobilization, 5′ overhangs generated after restriction were filled in with biotinylated nucleotides by Klenow (exo-) (New England Biolabs) as follows: 50 μM biotinylated dATP and/or dUTP (Life technologies, or Sigma, respectively) were combined with 200 μM of the remaining dNTPs (Bioline). To avoid degradation by nucleases in the extract, dTTP or dGTP were replaced by thio-dTTP or thio-dGTP (Enzo Life Sciences), respectively. Filled-in DNA was purified over G50 Sepharose columns (Roche) or the NucleoSpin Gel and PCR Clean-up kit (Macherey-Nagel). M-280 Dynabeads (Life Technologies) were washed once with PBS (+0.05% (v/v) BSA, 0.05% (v/v) NP40) and twice with 2× B&W buffer (2 M NaCl, 50 mM Tris-Cl pH 8.0, 1 mM EDTA). For immobilization, 30 ng/μl biotinylated DNA in 1× B&W buffer were added to at a ratio 30 μl slurry/1 μg DNA. Beads and coupling mix were incubated over night at 4°C while rotating. Linear DNA was immobilized either on one end (oeb) or on both ends (beb) (26). The completeness of these immobilization schemes was controlled by specific restriction cleavage.

Chromatin assembly and micrococcal nuclease digest

About 1 μg of DNA was added to 60 μl extract supplied with 10 mM 3-glycerophosphate (f.c.), and 12 μl of a 10x ATP-regenerating system (30 mM ATP, 300 mM creatine phosphate, 100 μg/ml creatine kinase, 30 mM $MgCl_2$, 10 mM DTT) and filled up to a total volume of 120 μl with EX50 buffer (10 mM HEPES, pH 7.6, 50 mM KCI, 1.5 mM $MgCl_2$, 0.5 mM EGTA, 10% glycerol, 10 mM 3-glycerophosphate; 1 mM DTT, 0.2 mM PMSF, 1 mM Aprotinin, 1 mM Leupeptin, 1 mM Pepstatin). Chromatin was assembled at 26°C. For MNase digestion 1.5 mM f.c. $CaCl_2$ and 1.4×10^{-3} units MNase were added and incubated at 30°C for 15 min. After quenching the reaction with 10 mM f.c. EDTA, samples were treated with 20 μg RNase A for 30 min. Proteins were digested overnight at 37°C after adding 16 μl 2% SDS and 100 μg Proteinase K.

Generation and characterization of Ku antibodies

Rat monoclonal antibodies were generated against Ku70 (Flybase: Irbp, FBpp0081861): Ku70-1: SEDEEDVSMK RDYHG, Ku70-2: QDWNNTENTADEQK and Ku80 (Flybase Ku80, FBpp0080322): Ku80-1: TLRDTQQPRP WAQN; Ku80-2: YDNDKEDKMLKDKN. Hybridoma clones expressing the most specific antibodies were established. Specificity and sensitivity of those antibodies was monitored by western blotting of extract, *in vitro*-assembled chromatin on DNA, S2 cell extract and S2 extract after RNA interference against Ku70 RNAi or Ku80 (Supplementary Figure S1E).

Antibodies and western blotting

Proteins were transferred onto nitrocellulose membranes for 90 min at 400 mA. Membranes were blocked in 5% BSA in TBS-T (25 mM Tris-Cl pH 8, 3 mM KCl, 140 mM NaCl, 0.1% Tween20) and incubated with primary antibody in TBS-T overnight at 4°C. The following antibody concentrations were used: 1:5 for rat αKu70 and αKu80 monoclonals, 1:5000 for rabbit αH2AvD pS137 (Biomol), 1:20 000 for rabbit αH3 antibody ab1791 (Abcam), WB 1:5000 for rabbit αH4 antibody ab10158 (Abcam).

Chromatin immunoprecipitation

Chromatin immunoprecipitation was performed on standard chromatin assembly reactions, unless indicated otherwise. Crosslinking was for 10 min at 26°C with 0.01% or 0.1% formaldehyde, for histones or chromatin remodelling factors, respectively. To capture fast spreading events, crosslinking was performed with 0.1% formaldehyde for 3 min at 26°C. Crosslinking was quenched by the addition of 125 mM glycine for 5 min at 26°C. Then, after addition of 1.5 mM $CaCl_2$, chromatin was fragmented by MNase treatment for 15 min at 30°C, with 1.2 U/μg DNA for chromatin assembled from endogenous nucleosomes, and 2.4 U/μg DNA for chromatin assembled from recombinant nucleosomes, respectively. MNase digestion was stopped with 10 mM EDTA, and RIPA (150 mM NaCl, 1.0% NP-40 or Triton X-100, 0.5% Na deoxycholate, 0.1% SDS, 50 mM Tris-Cl, pH 8.0) was added to 500 μl per 1 μg DNA. For pre-clearing 30 μl of a slurry of protein A or G beads washed with RIPA was added followed by the incubation for 1 h on a rotating wheel at 4°C. For monoclonal rat antibodies, protein G beads were washed with PBS and bound to antibody overnight on a rotating wheel at 4°C (1.5 ml antibody per 30 μl beads). Antibodies for immunoprecipitation were added to the supernatants of pre-clearing. Chromatin samples including the antibody were incubated overnight on a rotating wheel at 4°C, supplied with 30 μl protein A or G beads and incubated for 3 h on a rotating wheel at 4°C. Beads were washed five times with RIPA buffer, for 10 min each on a rotating wheel at 4°C and supplied with 100 μl TE including 10 μg RNaseA. After incubation of 30 min at 37°C while shaking, samples were supplied with 0.5% SDS and 100 μg proteinase K. Decrosslinking was performed at 68°C and 800 rpm for 2 h, followed by 37°C and 800 rpm overnight. DNA was then purified using the Genelute PCR Clean-Up Kit (Sigma) and eluted in 30 μl TE buffer.

Mass spectrometry

After assembly, beads were washed with EX50 buffer (w/o protease inhibitors) supplied with 2 mM DTT, and beads and input samples were filled up with the same buffer to 20 μl. Samples were incubated at 56°C for 35 min to reduce disulfide bonds and cooled to RT. Then 5 M urea in 100 mM Tris-Cl, pH 8.0 and 10 mM iodoacetamide (f.c.) was added and incubated for 35 min in the dark at RT while shaking. Samples were further diluted with 100 mM ammonium bicarbonate to a final concentration of 1 M urea. About 5 μg trypsin was added to each SN or input sample or 1 μg trypsin to each beads sample and incubated overnight at 30°C. Beads were then collected on magnets and supernatants were transferred to fresh vials. Beads were washed twice with 70 μl 0.2% formic acid (v/v) and supernatants from washing were combined with the previous supernatant from digestion. Samples were then acidified with trifluoroacetic acid to pH 2–3 and desalted with C18 stage tips. The eluate was vacuum dried, dissolved in 20 μl 0.2% (v/v) formic acid and analysed with LC MS/MS using the Triple TOF 6600 system (Sciex). In order to reduce the number of missing values generated by data-dependent acquisition, we decided to employ a nanoLC-SWATH-MS acquisition method with optimized SWATH window distribution depending on the precursor ion m/z distribution measured in previous chromatin assemblies. Therefore, the sample was loaded onto an in-house packed separation column (300 × 0.075 mm, packed with 2.4 μm C18 material, Reprosil-AQ, Dr Maisch AG). A linear gradient from 2 to 35% ACN over 100 min was applied to separate the peptide mixture, and the column outlet was directly coupled to the nano-ionization source of the 6600 Triple TOF mass spectrometer (Sciex). A SWATH-library was prepared from chromatin assemblies and is described in (27). Replicates were measured using a 40 window SWATH method ranging from 300 to 1200 m/z with window sized distribution according to precursor distribution in the library samples. Fragmentation energies (CID) for all fragmentation steps were optimized for 2+ precursors since they were the most abundant in the library. SWATH-data were matched to the library within the PeakView 2.2 software suit (Sciex) employing up to 6 peptide per protein and 5 fragments per peptide. Peptide detection was limited to a mass window of 40 ppm (±20 ppm) and after retention time recalibration to an elution window of 5 min around the expected peptide retention time. Peak areas were extracted using Marker View 1.4 (Sciex), and median normalization and statistical calculations were performed in R.

Phosphopeptide enrichment

Chromatin assembly reactions containing 1.5 mg extract protein (15 mg/ml) were sonicated for 10 min in a bioruptor (4°C) and treated with benzonase before acetone precipitation. Phosphopeptides were then enriched using the EasyPhos method as previously described (28). Briefly, protein pellets were resuspended in 500 μl TFE digestion buffer

and digestion enzymes (trypsin and LysC) were added in a 1:100 ratio (enzyme:protein). After overnight incubation at 37°C with rapid agitation (1500 rpm), aliquots for proteome analysis (10 μg) were taken. For phosphopeptide enrichment, a buffer containing 150 μl 3.2 M KCl, 55 μl of 150 mM KH_2PO_4, 800 μl 100% acetonitrile (ACN) and 95 μl 100% trifluoroacetic acid (TFA) was added to the peptides and incubated at RT for 5 min at 1600 rpm prior to centrifugation. After centrifugation, the peptide supernatant was incubated with TiO_2 beads (ratio 10:1; beads:protein solution) at 40°C for 5 min at 2000 rpm. Beads with bound phosphopeptides were pelleted by centrifugation for 1 min at 3500 *g* and the supernatant was discarded. Beads were then resuspended in wash buffer (60% ACN and 1% TFA), transferred to a clean 2 ml tube and washed further four times with 1 ml of washing buffer. After the last wash, beads were transferred to transfer buffer (80% ACN and 0.5% acetic acid) on top of C8 StageTips. After centrifugation phosphopeptides were eluted with 60 μl elution buffer (40% ACN and 15% NH_4OH [25%, HPLC grade]), collected in clean PCR tubes and concentrated in a SpeedVac for 15 min at 45°C. Peptides from the enrichment and from the total proteome were acidified with TFA (1% final concentration), concentrated and desalted using stageTips with two layers of styrene divinylbenzene-reversed phase sulfonated (SDB-RPS; 3M Empore). StageTips were washed twice with 0.2% TFA and once with isopropanol containing 1% TFA. Peptides were eluted by adding 60 μl SDB-RPS elution buffer [80% ACN, 1.25% NH_4OH (25% HPLC grade)] and immediately concentrated in a SpeedVac for 30 min at 45°C. Concentrated peptides were suspended in a buffer containing 2% ACN and 0.1% TFA prior to chromatography-tandem mass spectrometry (LC-MS/MS) analysis. For every condition (control, circular or linear DNA), four phospho-enriched and proteome replicates were prepared.

LC-MS/MS analysis for phosphopeptides and proteome

Phosphopeptides were loaded onto a 50 cm reversed-phase column (diameter 75 μM; packed in-house with 1.9 μM C18 ReproSil particles [Dr Maisch GmbH]; column oven temperature was set to 60°C). The column was mounted to an EASY-nLC 1200 system (Thermo Fisher Scientific). The peptides were eluted from the column with a gradient consisting of solution A (0.1% formic acid) and solution B (80% ACN and 0.1% formic acid). Gradient length was 130 min from 5 to 65% solution B with a flow rate of 300 nl/min. Peptides were analysed in a Q Exactive™ HF-X mass spectrometer (MS) (Thermo Fisher Scientific) coupled to the nLC, obtaining full scans (300–1600 m/z, $R =$ 60 000 at 200 m/z) at a target of 3e6 ions and maximum injection time of 120 ms. The 10 most abundant ions were selected and fragmented with higher energy collisional dissociation (HCD) (target 1e5 ions, maximum injection time 120 ms, isolation window 1.6 m/z, normalized collision energy 28%) followed by the detection in the Orbitrap ($R =$ 15 000 at 200 m/z). Proteome samples were measured with slight modifications using a 25 cm column, sequencing the 15 most abundant peptides and a maximum injection time of 28 ms for full scan acquisition. Raw MS data files were processed using MaxQuant (version 1.6.1.13) (29) with the Andromeda search engine with FDR < 0.01 at protein, peptide and modification level. The default settings were used with the following modifications: variable modification methionine (M), acetylation (protein N-term), as well as phospho (STY) and the fixed modification carbamidomethyl (C) were selected, only peptides with a minimal length of seven amino acids were considered. Peptide identification was done using the FlyBase (dmeI-all-translation-r6.25).

Statistical analysis of proteome and phosphoproteome

For immobilized chromatin, contaminants and reverse hits were removed, mass spectrometry protein intensity values were log2-transformed, median-normalized and proteins with low intensity values were filtered out. Biological replicates were analysed by principal component analysis, and biological replicates identified as outliers (oeb_3h_2, oeb_3h_3, beb_3h_2, beb_3h_3) were omitted in further analyses. For the phosphoproteome, contaminants and reverse hits were removed from phosphorylated peptide lists. Only phosphopeptides detected in 2 of 4 biological replicates were considered. Normalized phosphopeptide intensities were log2 transformed. Statistical tests for immobilized chromatin and for the phosphoproteome were performed with empirical Bayes moderation using the limma R package (version 3.34.9). Scatterplots and volcano plots were generated using R base graphics, and heat maps were plotted by using the pheatmap R package (version 1.0.10).

GO term analyses were performed with PANTHER version 14.0 (released 12 March 2018, Panther Go-Slim Biological Process for immobilized chromatin or GO cellular component complete for phosphoproteome, Reference List: *Drosophila melanogaster*, Test Type: Fisher's Exact).

ChIP qPCR and sequencing

MNase-cleaved DNA after overnight proteinase K digestion was purified with the GenElute PCR clean-up kit (Sigma-Aldrich). For qPCR, DNA was quantified by LightCycler 480 Instrument II with reference to a standard curve of input DNA. Libraries for single-end sequencing were prepared using the MicroPlex Library Preparation kit (Diagenode). Fifty base pair sequencing reads were obtained on a HiSeq 1500 (Illumina) instrument. Reads were aligned to the reference genome (version dm6) using bowtie2 (version 2.2.9). Coverage vectors were generated from BAM files using R/Bioconductor packages, and were normalized to the total number of reads derived from the uncut fosmid. Tracks were exported as Bedgraph files and visualized in IGV browser (version 2.3.79).

Histone expression and reconstitution of nucleosome arrays

Nucleosome arrays were reconstituted by salt gradient dialysis of recombinant *Drosophila* histones and either plasmid DNA or fosmid DNA. Histones were purified as described earlier (30) with the following modifications: due to the lower pI, histone H2A.V and its tagged versions were purified in buffer Sau-0 instead of Sau-200. Histone H3 and H4 were kind gifts from Dr C. Regnard (prepared by the purification of inclusion bodies). For octamer reconstitution, ratios of the corresponding histones were titrated

to reach final ratios of H2A:H2B:H3:H4 1.2:1.2:1:1. After titration, histones were pooled, lyophilized and resuspended in unfolding buffer to final concentrations of 4.7 mg/ml for H2A and H2B, and 4.0 mg/ml for H3 and H4, respectively. The histones were dialyzed against refolding buffer at 4°C overnight. Octamers were purified by size exclusion chromatography in refolding buffer on a Hiload 16/600 Superdex 200 column (Sigma).

Each 100 μl assembly reaction containing DNA, histones, 20 μg BSA, 0.1% Igepal CA-630, 10 mM Tris-Cl pH 7.6, 2 M NaCl and 1 mM EDTA were transferred to dialysis cups (Slide-A-Lyzer; MWCO 3500, Thermo Fisher). The dialysis cups were floated in a beaker containing 300 ml high salt buffer (10 mM Tris-Cl pH 7.6, 2 M NaCl, 1 mM EDTA pH 8.0, 0.05% Igepal CA-630, 0.1% 2-mercaptoethanol). The NaCl concentration in the beaker was decreased constantly at RT over night by pumping 3 L of low salt buffer (10 mM Tris-Cl pH 7.6, 50 mM NaCl, 1 mM EDTA, 0.05% Igepal CA-630, 0.01% 2-mercaptoethanol) into the beaker with a peristaltic pump (Minipulse evolution, Gilson, mode 8.4 rpm). After the entire low salt buffer had been transferred, the dialysis cup was dialysed for another 2 h at RT against fresh low salt buffer. The quality of nucleosome assembly was assessed by limited MNase digestion.

RESULTS

Selective marking of damaged DNA by H2A.V phosphorylation in reconstituted chromatin

Chromatin assembled in preblastoderm *Drosophila* embryo extract ('extract' from hereon) displays nucleosomes with physiological spacing, revealed by partial digestion with Micrococcal nuclease (Supplementary Figure S1A) (7). Preblastoderm embryos contain large stockpiles of H2A/H2B and H2A.V/H2B dimers bound to lipid droplets (31). To test whether H2A.V was incorporated into chromatin, we coupled linear DNA to paramagnetic beads (32), assembled it into chromatin, retrieved the immobilized chromatin from the extract and probed for the presence of H2A.V by western blotting (Figure 1). H2A.V was detected as a prominent band in the extract and on chromatin. In several replicates, the antibody detected a fainter band migrating slower than the unmodified H2A.V. The electrophoretic mobility suggests that this band corresponds to the γH2A.V phosphoform. This was confirmed by probing the blots with an γH2A.V antibody (Figure 1B).

To explore the circumstances that lead to H2A.V phosphorylation, we assembled chromatin on linear or circular plasmid DNA, or on linear DNA immobilized to paramagnetic beads by a biotin-streptavidin linkage and probed for the presence of the phospho-form (Figure 1A and B). In the absence of DNA, H2A.V was not phosphorylated. On chromatin assembled on circular DNA, low levels of γH2A.V were detected that may originate from background levels of DNA damage introduced during preparation (Figure 1A; lanes 1 and 3). However, in presence of linear DNA, either free or immobilized on beads, ∼30–50% of incorporated H2A.V became phosphorylated (lanes 4, 6 and 7). In lanes 4 and 7, excess unphosphorylated H2A.V present in the extract was not separated from nucleosomal H2A.V leading to a higher fraction of unphosphorylated H2A.V.

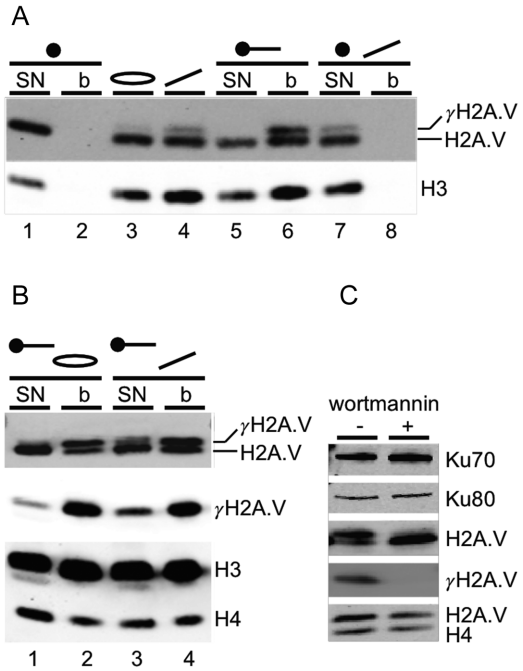

Figure 1. Detection of γH2A.V on chromatin with free ends. (**A**) Western blot analysis of *in vitro*-reconstituted chromatin on linear (lanes 4, 7 and 8) or circular DNA (lane 3) in solution, or on linear DNA coupled to paramagnetic beads (black circle) with one end (lanes 5 and 6). γH2A.V runs slightly slower than H2A.V. In the absence of DNA, no H2A.V phosphorylation occurs (lanes 1 and 2). Membranes were probed with antibodies against H2A.V and H3. SN: supernatant after magnetic retrieval of the beads; b: beads isolated from extract on the magnet. (**B**) Western blot as in panel (A) probing chromatin assembly reactions containing linear bead-bound chromatin and free circular or linear DNA with antibodies specific for the indicated proteins. (**C**) Western blot as in panel (B) probing chromatin assembly in the absence or presence of wortmannin, a broad-range PI3K inhibitor. Addition of the solvent, DMSO, served as negative control.

To test for the specificity of γH2A.V for DNA with free ends (a proxy for a broken chromosome), we assembled chromatin on bead-bound linear DNA along with soluble circular or linear DNA in the same reaction. After separating immobilized DNA from the DNA and excess H2A.V in the supernatant, the phosphorylation status of H2A.V on beads and in the supernatant was analyzed (Figure 1B). The γH2A.V signal exceeded background levels only on beads with coupled DNA (lanes 2 and 4, for a negative bead-only control see Figure 1A), or in the supernatants containing linear, but not circular chromatin (compare lanes 1 and 3, Figure 1B). Apparently, the break-induced phosphorylation remains confined to linear chromatin and does not 'spread' to circular chromatin in the same reaction. H2A.V phosphorylation could be prevented by including wortmannin, a broad-range PI3K inhibitor (33), in the assembly reaction (Figure 1C).

Reconstituted *Drosophila* preblastoderm embryo chromatin contains DNA repair factors

The observation of γH2A.V phosphorylation on DNA with an unprotected end suggests that the extract-assembled chromatin contains sensors and mediators of the DNA

damage response. To test for the recruitment of such proteins to free DNA ends, linear DNA that was bound to paramagnetic beads either at one end ('one end bound', oeb) or at both ends ('both ends bound', beb) [Figure 2A and (26)]. Chromatin assembly proceeded equally on both types of DNA (Supplementary Figure S1B). The chromatin proteins on either immobilized DNA were analysed by mass spectrometry. Paramagnetic beads lacking DNA served as control for unspecific protein binding. The intensity values obtained from this control were subtracted from the protein intensities obtained from the DNA beads and compared in Figure 2B. Proteins on the left bottom quadrant are mainly found in the control samples and are mostly ribosomal proteins (data not shown) (34,35).

Among the 349 chromatin-associated proteins (Figure 2B and Supplementary Table S1, with positive coefficients for oeb versus control and beb versus control), we identified many proteins with the GO terms relevant to our interest, with *P*-values given in brackets: DNA-dependent DNA replication (1.83E-05), chromosome condensation (2.46E-10), meiotic nuclear division (1.01E-02), mitotic spindle organization (2.05E-02), DNA biosynthetic process (1.18E-05), protein import into nucleus (3.67E-03), protein–DNA complex assembly (6.08E-03), protein ubiquitination (1.62E-11), DNA repair (1.21E-04), chromatin organization (5.51E-03) and proteasome-mediated ubiquitin-dependent protein catabolic process (1.45E-03). All identified proteins are shown in Figure 2B according to their enrichment on oeb (*x*-axis) or beb (*y*-axis) assembly reactions over control and listed in Supplementary Table S1. Among those, all proteins associated with DNA damage are shown in Supplementary Figure S1C. The top-10 proteins associated with DNA damage and with the highest enrichment on oeb over control are highlighted in orange (Figure 2B) and listed in Figure 2C. These include proteins of the HR pathway, such as components of the MRN complex (mre11 and Rad50) and the RPA complex (Replication Protein A complex, consisting of Rpa-70, RPA2 and RPA3). RPA is the major ssDNA-binding protein complex during DNA resection (36). We also found proteins of the non-homologous end joining (NHEJ) pathway (Ku70/Irbp and Ku80). In addition, Rrp1 (recombination repair protein 1), an enzyme whose activities include AP-endonuclease, 3′-exonuclease, 3′-phosphodiesterase and 3′-phosphatase (37,38), was also identified on immobilized chromatin. Canonical histone proteins and the histone variant bigH1 were enriched on chromatin (39), but without any preference for oeb or beb (Supplementary Table S1). In contrast, H2A.V showed a slight enrichment on oeb (Figure 2B and Supplementary Table S1).

The intensities of most DSB-associated proteins were not enriched with statistical significance on oeb DNA versus beb DNA, which had been designed to block both ends (26). Apparently, this blockage was incomplete. While Ku was occluded by the streptavidin–biotin linkage, beb chromatin still collected γH2A.V, showing that the end was recognized by damage recognition factors (Figure 2E). Conceivably, the end may still be accessible given the long linker connecting biotin to the base. Alternatively, the bulky adduct itself may trigger the damage response (see 'Discussion' section). It is therefore possible that some recruitment of DNA damage factors to beb may be through by interactions with γH2A.V.

To explore the kinetics of factor recruitment to oeb and beb DNA, the mass spectrometry analysis was repeated with seven biological replicates and at early (15 min) and late (3 h) assembly times (Figure 2D; Supplementary Figure S1D and Supplementary Table S2). We found the Ku complex significantly enriched at both time points on oeb DNA, confirming its known specificity for unprotected DNA ends. In addition, we found the RPA complex substantially enriched on oeb DNA after 3 h, but not after 15 min.

Ku70 (named Irbp in *Drosophila*) and Ku80 (40,41) were found particularly enriched on oeb DNA, presenting a free end, at the earliest time point (Figure 2D). To confirm this observation, we raised monoclonal antibodies against Ku70 and Ku80. Although the antibodies cross-react extensively with cytoplasmic proteins, they detect specific signals of the right size in purified chromatin (Supplementary Figure S1E). The corresponding bands are reduced if the Ku70 and Ku80 proteins are depleted by RNA interference in S2 cells, indicating their suitability for chromatin analyses (Supplementary Figure S1E). Western blot analysis during a time course of chromatin assembly showed that Ku70 associated with DNA ends already after 2 min of incubation in extract and remained on chromatin throughout the 2-h reaction. This fast binding precedes the formation of nucleosomes, which was reflected by the constant increase of H2A.V between 2 and 120 min (Figure 2E).

In summary, our proteomic analysis detected numerous proteins involved in various aspects of DNA damage response. Among the proteins involved in the repair of DSBs, we detected key factors involved in the recognition and processing of DSBs: the Ku70/80, MRN and RPA complexes.

Ku binding and resection

Ku70 was recruited in response to free DNA ends independent of γH2A.V (Figures 1C and 2E), in line with previous observations (3,42,43). We wished to visualize the interaction of the Ku complex with break sites by chromatin immunoprecipitation (ChIP). To increase the spatial resolution, we assembled chromatin on fosmid DNA (24). These fosmids carry on average 36 kb of *Drosophila* genomic DNA in a 10 kb vector. In these reactions, we assembled two arbitrarily chosen fosmids with different *Drosophila* genomic sequences. FlyFos019829 (termed fosmid 'B' further-on) was included as an intact circle and served as undamaged control. FlyFos019611 (termed fosmid 'A') was added either in its circular form (control) or cut by FseI (cut, Figure 3). Early during the assembly (10 min), Ku proteins were specifically enriched close to the FseI cut site. This recruitment was verified by ChIP-qPCR (Supplementary Figure S2A and B). The enrichment was no longer detected after 2 h, even though Ku remained bound to the DNA fragment with the free end for at least this time (Figure 2E). It is possible that the ring-shaped Ku complex slides away from the end to heterogeneous, more internal positions during extended incubation (42,44). It is also possible that the Ku complex associates with single-stranded (ss) DNA (45), which was not detected in ChIP-seq.

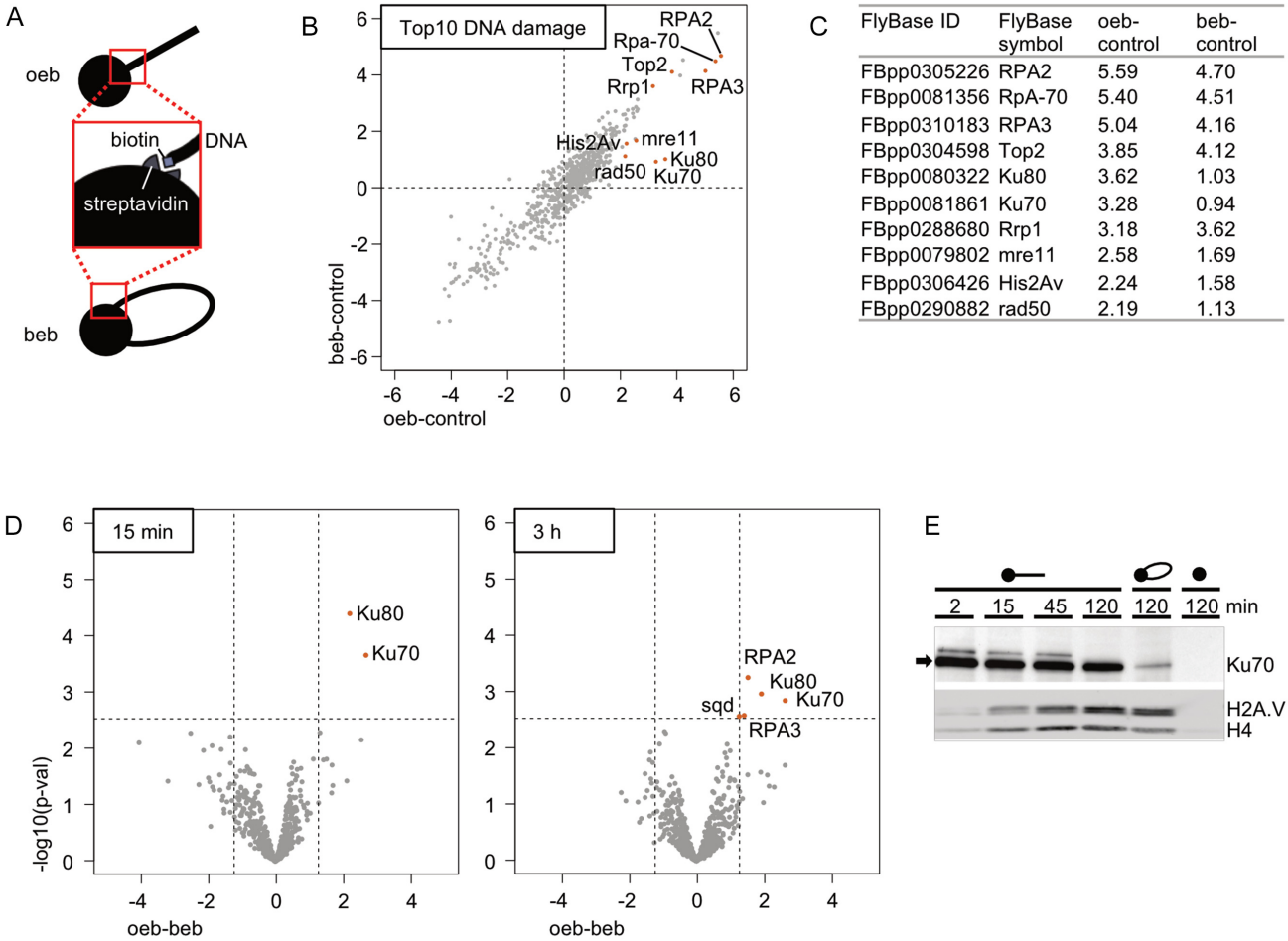

FlyBase ID	FlyBase symbol	oeb-control	beb-control
FBpp0305226	RPA2	5.59	4.70
FBpp0081356	RpA-70	5.40	4.51
FBpp0310183	RPA3	5.04	4.16
FBpp0304598	Top2	3.85	4.12
FBpp0080322	Ku80	3.62	1.03
FBpp0081861	Ku70	3.28	0.94
FBpp0288680	Rrp1	3.18	3.62
FBpp0079802	mre11	2.58	1.69
FBpp0306426	His2Av	2.24	1.58
FBpp0290882	rad50	2.19	1.13

Figure 2. Enrichment of DNA damage-associated proteins on *in vitro* reconstituted chromatin. (**A**) Schematic illustration of immobilization of linear DNA with one biotinylated end (oeb) or both ends (beb) to streptavidin-coated paramagnetic beads. (**B**) Proteins detected on immobilized DNA by mass spectrometry after 4 h of assembly. After normalization, log-transformation and subtraction of bead control, relative enrichments of proteins found on the oeb fragment (*y*-axis) were plotted against the relative enrichment on the beb fragment (*x*-axis). The diagram represents the averaged values of three biological replicates (extract preparations). The 10 proteins with highest enrichment on oeb over control and associated with the GO term DNA damage (top-10) are highlighted in orange. (**C**) The top-10 DNA damage-associated proteins enriched on oeb and highlighted in panel (B) are listed with their Flybase polypeptide ID. Proteins are sorted according to their enrichments on oeb relative to control. (**D**) Volcano plot with -log10 *P*-values (*y*-axis) and log fold-difference (*x*-axis) after comparison of chromatin-associated factors on oeb versus beb DNA. Intensities were measured by mass spectrometry after 15-min assembly (left) and after 3 h assembly (right). The 15-min assembly values are averaged intensities from seven biological replicates, the 3-h value consists of averaged intensities from five biological replicates. (**E**) Western blot revealing the time course of association of Ku70, histone H2A.V and histone H4 to *in vitro*-reconstituted chromatin on oeb DNA. About 120-min time points with beb chromatin or beads lacking DNA serve as reference. Chromatin assembly proceeded for 2 to 120 min as indicated.

We consistently observed a loss of DNA close to the cut sites upon extended incubation in the assembly reaction, which is seen as a dip in sequencing read coverage in ChIP-seq tracks, including the input (Figure 3). Conceivably, this loss of DNA could be due to MNase digestion after removal of nucleosomes by nucleosome remodellers (46,47). To explore this possibility, we fragmented the chromatin for ChIP with adaptive focused acoustics (Covaris) instead of MNase and still observed a similar loss of ∼3 kb of DNA flanking the break point (Supplementary Figure S2C). Therefore, given the specific association of the ssDNA-binding RPA complex in our MS survey at these late times, this finding points to resection-type reactions in our extract (Figure 2D). Resected, ssDNA is not represented in the sequencing libraries.

Spreading of the γH2A.V signal in *cis* from the DNA break

Chromatin assembly on linear and circular DNA in the same reaction had suggested that the γH2A.V signal remained confined to the DNA bearing unprotected ends and did not spread to DNA circles (Figure 2B). When we monitored the distribution of γH2A.V on cut relative to uncut fosmid DNA, we found the entire cut fosmid A covered with the phosphorylation mark already after 10 min of incubation in the extract, while phosphorylation of similar levels of H2A.V on the circular fosmid B was much lower, confirming the previous observation that H2A.V phosphorylation does not spread in *trans* (Figure 3). Apparently, the extract supports fast spreading of the γH2A.V mark along many kilobases of DNA in a short time.

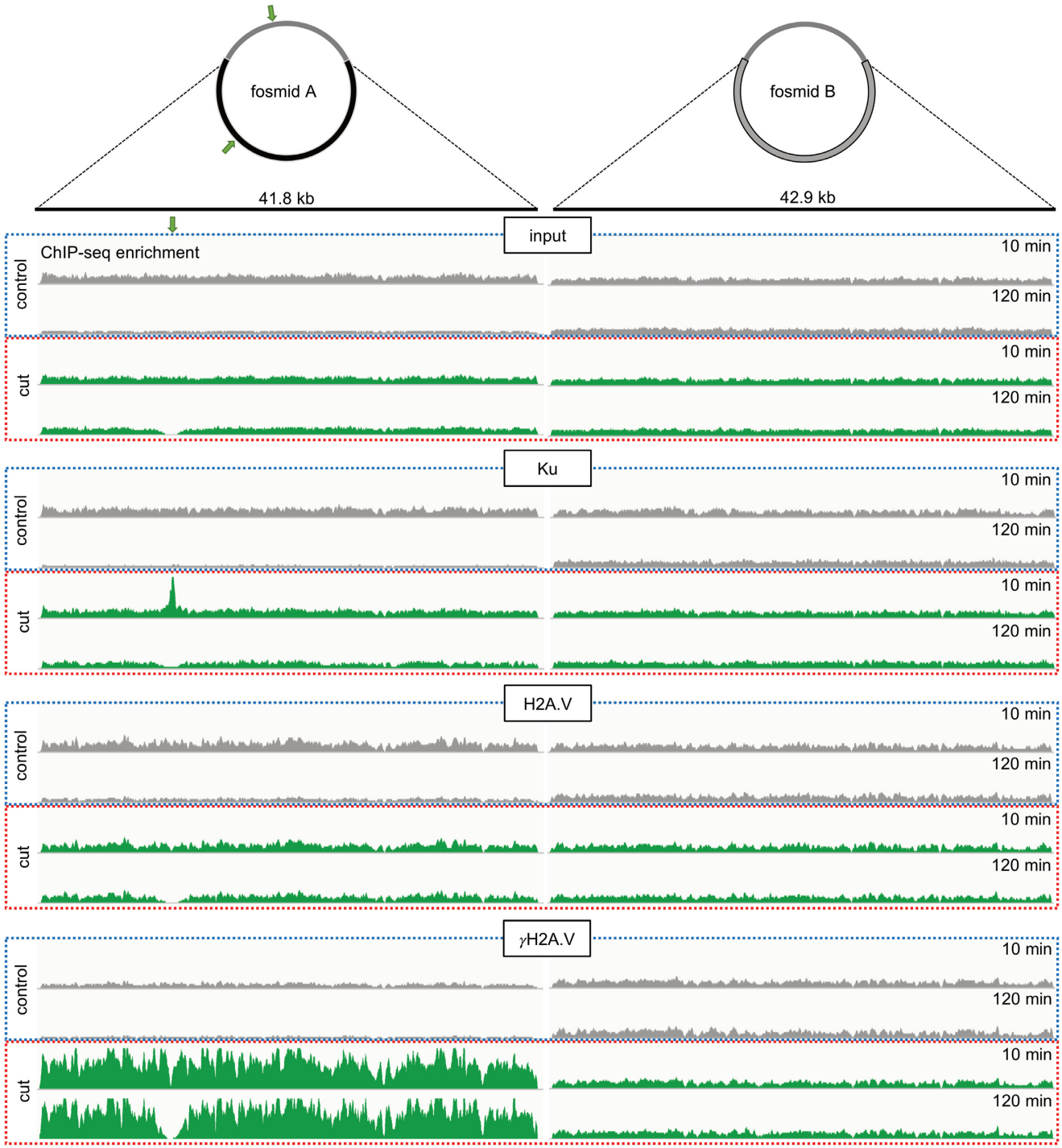

Figure 3. Visualization of Ku binding and H2A.V phosphorylation on DNA with free ends. ChIP-Seq on chromatin assembled for 10 or 120 min on a mix of circular control fosmid B and on fosmid A, which was either circular (control, blue box) or cleaved by restriction with FseI (cut, red box). ChIP was done with antibodies against the Ku complex (using a mixture of Ku70 and Ku80 monoclonal antibodies), H2A.V and γH2A.V. Green arrows indicate the FseI cleavage sites in fosmid B. Reads were normalized to the control fosmid B. The mapped region on the fosmid is indicated with dashed lines and spans a region of ∼40 kb.

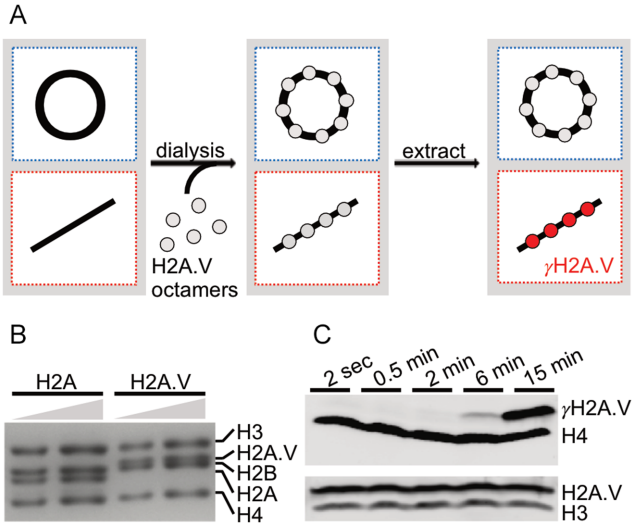

Figure 4. Studying γH2A.V phosphorylation on recombinant nucleosome arrays. (**A**) Schematic illustration of the experimental design. Nucleosome arrays were reconstituted on circular control DNA or cut DNA by salt gradient dialysis. These arrays were then incubated in extract. In this way, nucleosome assembly and fast H2A.V phosphorylation can be disentangled. (**B**) Two amounts of recombinant octamers containing either H2A or H2A.V were separated by SDS-PAGE and stained by Coomassie. (**C**) Western blot probing H2A.V phosphorylation on linear fosmids after 2 s, 0.5, 2, 6 and 15 min. Membranes were probed with the indicated antibodies.

Such spreading of γH2A.V phosphorylation has, to the best of our knowledge, so far not been observed *in vitro*. This observation presents a unique opportunity to study the process of γH2A.V spreading in a cell-free system amenable to biochemical manipulation. Remarkably, the development of the γH2A.V signal was very fast, mirroring the kinetics of nucleosome assembly in this system (7). To disentangle the kinetics of γH2A.V spreading from the nucleosome assembly process, we reconstituted H2A.V-containing nucleosome arrays from recombinant histones. Recombinant histones were expressed in *Escherichia coli* and refolded with the other histones into histone octamers [Figure 4A and B (30,48)]. The octamers were mixed with DNA in high salt, and nucleosomes were formed by salt gradient dialysis. In a pilot experiment, we assembled fosmid DNA into H2A.V-containing nucleosome arrays. When this substrate was incubated in extract, the γH2A.V signal could be detected by western blotting after ∼6 min (Figure 4C).

Next, we assembled H2A.V-containing nucleosome arrays on fosmids A and B by salt gradient dialysis and incubated them in extract under assembly conditions to capture the rapid spreading of γH2A.V. Monitoring γH2A.V on western blots showed background levels on control DNA, which may be due to DNA shearing during fosmid preparation, and an increase in bulk phosphorylation between 2 and 10 min, if fosmid A was linear (Figure 5A). To observe spreading of H2A.V phosphorylation from different locations, we cleaved fosmid A with FseI (which cuts once in the genomic insert and once in the vector backbone) as before or RsrII (which cleaves the insert twice). In the control reaction, both fosmids were intact and no γH2A.V was detected (Figure 5B). On the cleaved fosmids, the increase of γH2A.V was obvious after 10 min, whereas no phosphorylation was detected in control fosmid B. The γH2A.V signal covered the entire fosmid inserts, but showed a clear gradient of intensities around the respective cut sites, in the ChIP seq profiles and the corresponding qPCR validation (Figure 5B). As a further variation of the experiment, we swapped 'control' and 'experimental' fosmid: we kept fosmid A intact and cleaved fosmid B with SgrDI (one target site in the genomic insert, marked with a grey arrow in Figure 5B). Quantitative PCR reveals elevated levels around this site, while the amplicons on fosmid A showed no increase (Figure 5C). Collectively, these experiments revealed fast spreading of the γH2A.V signal from unprotected DNA ends over minimally 10 000 base pairs in our cell-free system.

Identification of DSB-dependent phosphorylation sites

The robust phosphorylation of H2A.V indicates that DNA damage-dependent phosphorylation is reconstituted in our *in vitro* system. To explore the extent of canonical damage signalling and identify phosphorylated target proteins, we enriched phosphorylated peptides for identification and quantification using MS-based quantitative phosphoproteomics. The experiment involved three reactions: (i) 'mock' chromatin assembly reactions without DNA, (ii) assembly reactions containing intact, circular plasmid DNA and (iii) assembly reactions containing linearized plasmid DNA. The experiment was performed in four biological replicates, i.e. involving four different chromatin assembly extracts. In total, 13 408 phosphorylated peptides matching to 2397 proteins were detected and quantified (see Supplementary Table S3). Interestingly, unsupervised clustering of the top 100 DNA-dependent phosphorylation events (Figure 6A) yielded distinctive clusters. Phosphorylated peptides in cluster 1 are related to the assembly system in the absence of DNA and are reduced upon addition of DNA. Cluster 2 only consists of phosphorylation of the uncharacterized protein encoded by CG42232 that is particularly abundant in the presence of circular, but not linearized DNA. Cluster 3 shows phosphorylated peptides with increased intensities upon addition of DNA, independent of topological state. The intensities of phosphorylated peptides in cluster 4 increased when DNA had unprotected ends. The list of all phosphorylation changes (Supplementary Figure S3A and Supplementary Table S3) serves as a useful resource for further analysis. For our current study, we focused on those phosphorylations that were significantly enriched in the presence of linear versus circular DNA. We found phosphorylated residues from 69 proteins that are significantly increased (linear-closed>0; -log10(p-val)>2) in a DNA end-dependent manner (Figure 6B and Supplementary Figure S3B). GO term analysis revealed remarkable enrichments of protein known to bind unprotected chromosome breaks or mitotic spindles (Figure 6C).

With our standard methods and settings, we did not identify the phosphorylated C-terminal peptide of H2A.V. There may be several reasons for this, including low abundance in the extract or a second, unknown modification of the peptide. Of note, even the unmodified peptide was identified only in a few replicates and with low intensity indi-

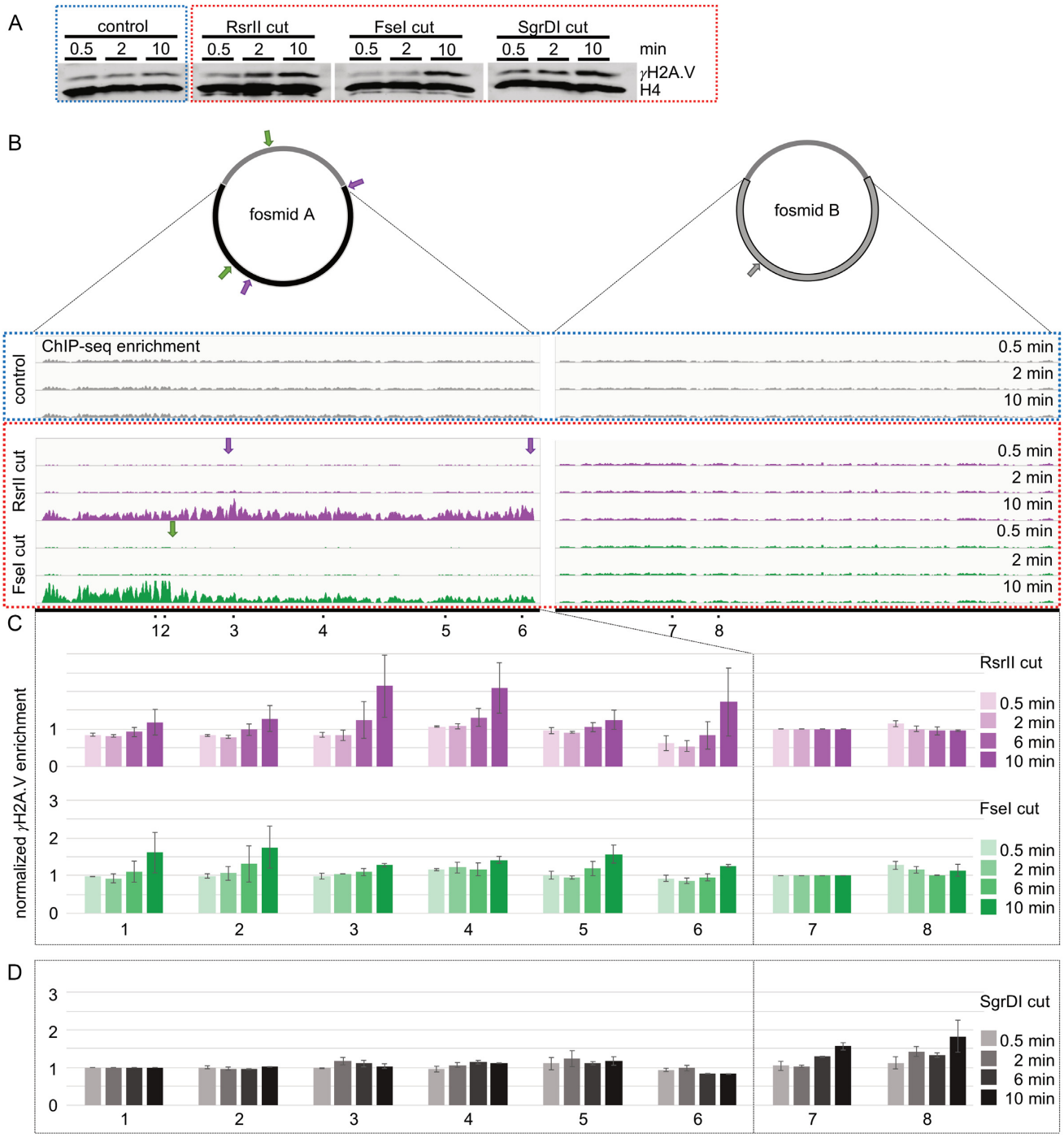

Figure 5. Time course of H2A.V phosphorylation. (**A**) Western blot visualizing the appearance of γH2A.V phosphorylation on pre-assembled fosmids. The reactions contain mixes of two fosmids, which either are both circular (control) or one of them is linearized by the indicated restriction enzymes. These DNAs were incubated in the extract for the indicated times and proteins were analysed by Western blotting. (**B**) H2A.V nucleosomes were reconstituted on fosmids A and B by salt gradient dialysis. Nucleosomal circular fosmid B and cleaved fosmid A (with either RsrII or FseI) were mixed and incubated in extract. After the indicated times, the reaction was stopped by formaldehyde crosslinking and samples were processed by MNase digestion and ChIP using H2A.V and γH2A.V antibodies. Top panel: γH2A.V ChIP-seq tracks on fosmid inserts after normalization to the control fosmid. The right part shows the circular fosmid B, which serves as an internal control. The left part shows the fosmid A, which had been cleaved by either RsrII (pink) or FseI (green) as indicated by the arrows. In the control reaction, both fosmids remained circular. Reads were normalized to the control fosmid B. (**C**) The same samples were subjected to ChIP-qPCR analysis for γH2A.V phosphorylation with amplicons probing 6 sites on fosmid A and 2 sites on fosmid B, as indicated (1–8). Percentage of input was determined and normalized to H2A.V and the control region 1 of the control fosmid. The experiment was performed in two biological replicates for FseI and four biological replicates for RsrII. Error bars indicate standard error of the means. (**D**) As a further control, the experiment described in panels (A) and (B) was repeated, but this time fosmid A remained intact and fosmid B was cleaved with SgrDI. For these samples no ChIP-seq tracks are shown, but only the ChIP-pPCR values. The data represent the mean of two biological replicates.

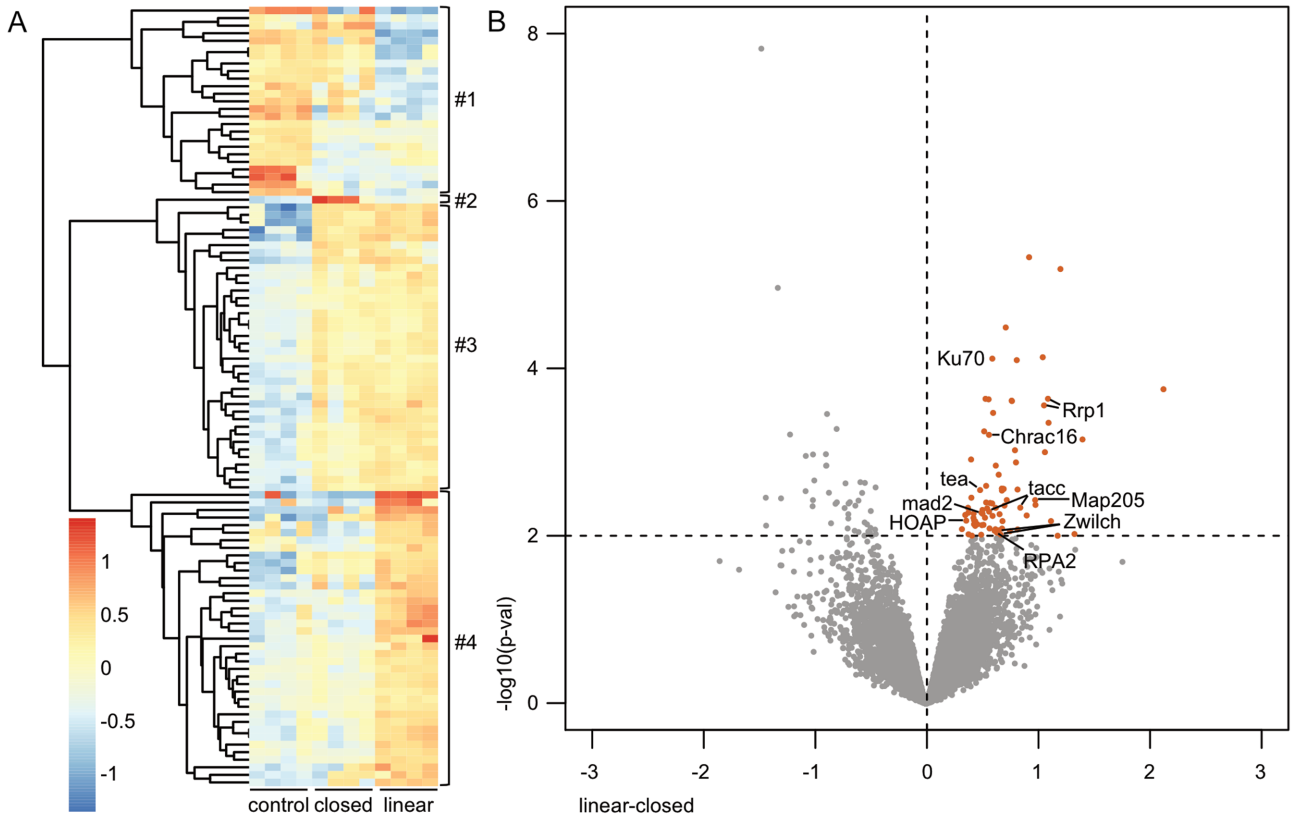

C

GO term (cellular component)	# of proteins (total: 69)	expected	fold enrichment	p-value
chromosome, telomeric region	4	0.2	25.7	2.25E-02
spindle	6	0.6	10.9	2.02E-02
polytene chromosome	8	1.0	7.9	7.93E-03
chromatin	9	1.4	6.2	1.34E-02
nuclear chromosome	8	1.3	6.1	4.57E-02
protein-containing complex	29	13.8	2.1	2.41E-02

Figure 6. Detection of phosphorylated peptides in the absence of DNA or in the presence of circular or linearized DNA by mass spectrometry. (**A**) Heat map showing relative enrichment of the top-103 phosphorylated peptides in the absence of DNA (control), in the presence of circular DNA (closed) or in the presence of linearized DNA (linear) performed in four biological replicates. The top-103 phosphopeptides were selected based on a *P*-value threshold of 0.001 in at least one of the three possible comparisons: closed versus control, open versus control, open versus closed. Four clusters formed by hierarchical clustering are indicated. Names of clustered phosphopeptides can be found in Supplementary Figure S3A and Supplementary Table S3. (**B**) Volcano plot with −log10 *P*-values (*y*-axis) and log fold-difference (*x*-axis) after comparison of phosphorylated peptides on linear versus circular DNA. The diagram represents the averaged values of four biological replicates (extract preparations) of phosphopeptides, which were identified in at least two of four biological replicates. Significantly enriched phosphopeptides on linear versus circular DNA (highlighted in orange) are listed in Supplementary Figure S3B. Phosphopeptides of proteins discussed in this chapter are labelled with their Flybase symbol. (**C**) GO term analysis of 69 proteins with phosphorylated peptides significantly increased in linear to circular DNA (see Supplementary Figure S3B).

cating that this peptide might not be well suited for electrospray ionization. This C-terminal peptide lacks the usual positive charge of a typical tryptic peptide and in case of phosphorylation the peptide will gain an additional negative charge, rendering it unlikely to be detected.

To illustrate the potential of our phosphopeptide list as a resource, we highlighted several proteins that may be directly involved in either canonical or syncytial DSB signalling (Figure 6B). The histone-fold protein CHRAC16 (49), which we find phosphorylated at serine 6 in the N-terminal 'tail' domain, is a small subunit of the Chromatin Accessibility Complex (CHRAC), a nucleosome remodelling complex that induces nucleosome sliding and that was originally purified from the extract (11). The dimerization partner of CHRAC16, CHRAC14, is a subunit of DNA polymerase ε that is involved in the DNA damage response (50). The human CHRAC complex has been shown to cooperate with the Ku70/80 complex for binding to chromosomal breaks (51).

One of the most robust events was phosphorylation of the Ku70 subunit Irbp at serine 313. The homologous Ser314 in mouse is part of a patch of amino acids that may be phosphorylated to induce the dissociation of Ku from the DNA to initiate resection and HR (52). Conceivably, Ku binds early, but is then phosphorylated during further incubation in the extract, giving way to exonuclease activity and RPA binding (Figure 2D). We observed phosphorylation of the RPA2 subunit at Ser174. The significance of this phospho-

mark is unclear at present. We also detect already known phospho-epitopes in the very N-terminus of RPA2, where they are involved in the DNA damage response in multiple ways (53).

Interestingly, the presence of DNA ends also correlates with phosphorylation of Rrp1, which we already detected as a chromatin-enriched DNA damage factor (Figure 2B and C). Conceivably, this exonuclease may contribute to the observed loss of DNA at free ends (Figure 3 and Supplementary Figure S2C). DNA ends with single-stranded overhangs resemble telomers in some respects and are therefore subject to the telomere capping machinery. Tea (telomere ends associated) is a recently identified subunit of the MTV complex that binds to single-stranded telomere DNA to prevent their fusion (54). We find not only tea phosphorylation stimulated by free ends, but also modification of the HOAP protein (encoded by the *caravaggio* (*cav*) gene), which is also required for telomere capping (55). This fits well the earlier finding that the MRN complex, which we see bound to DNA ends, is involved in telomere protection (56,57).

Conceivably, not all free, single-stranded ends in our *in vitro* system are properly capped by MTV and HOAP. Such unprotected 'telomer-like' ends activate not only the damage response, but also the spindle assembly checkpoint (SAC) (58). Remarkably, we found two components of the SAC in flies, Zwilch and mad2, phosphorylated in the presence of DNA ends. Zwilch participates as part of the Rod-Zw10-Zwilch in recruiting dynein and mad2 to kinetochores, and its absence leads to lagging chromosomes (59). Finally, dTACC and Map205 that may be involved in the centrosomal side of the SAC were found phosphorylated. The presence and phosphorylation status of both microtubule-associated proteins affect centrosome integrity, microtubule assembly as well as recruitment of polo-like kinase to microtubules (60). Hyperphosphoryation of dTACC leads to unstable mitotic spindles (61). These latter findings suggest that some aspects of the response of preblastoderm embryos may be reconstituted *in vitro*.

DISCUSSION

DSB recognition in reconstituted *Drosophila* preblastoderm chromatin

We discovered that chromatin assembly extracts from preblastoderm *Drosophila* embryos contain factors that recognize and bind to unprotected DNA ends and mount checkpoint responses, witnessed by phosphorylation of the histone variant H2A.V at its C-terminus and of several other proteins that may be involved in the physiological signalling of cleavage-stage embryos. The γH2A.V signal, analogously to the γH2A.X signal in mammals (18,62), is propagated within minutes in *cis* from the DNA end over the entire chromatin fragment, which in our case exceeded 10 000 bp. To our knowledge, this is the first observation of such extensive spreading of the damage signal in an *in vitro* system.

In *Drosophila*, like in other organisms, the choice of the repair pathway between non-homologous end joining (NHEJ) or homologous recombination (HR) is highly regulated (41,63). Repair by NHEJ, the preferred pathway in the G1 phase, is initiated by the recruitment of the DNA-dependent protein kinase (DNA-PK) complex consisting of the Ku70/Ku80 heterodimer and the kinase subunit. In *Drosophila,* the Ku complex consists of Irbp and Ku80, but the catalytic DNA-PK subunit has been lost (40,41). The end-processing nucleases or polymerases are not known. In NHEJ, the processed ends are ligated by a complex of ligase 4, XRCC4 and XLF, which have all been identified in *Drosophila* [reviewed in (41)]. HR is the preferred method for DSB repair in the presence of sister chromatids, i.e. in S/G2. In mammalian HR, the end is recognized by the CtIP–MRN complex (Mre11, Rad50 and Nbs1), which initiates resection of DNA ends. Resection is extended by the exonucleases, Exo1 and Dna2, leading to long 3′ overhangs (64), which are immediately bound by single-strand-binding RPA complex (65) and subsequently by Rad51 (spn-A, in *Drosophila*) (41). Orthologues of the MRN and RPA complexes, Exo1 and Dna2, and a candidate CtIP orthologue have been identified in *Drosophila* (41).

We detected many proteins known to be involved in DNA damage responses bound to reconstituted chromatin. Remarkably, we found the Ku70/80, RPA and MRN complexes enriched at unprotected ends. However, some of the observed enrichments were not very strong, presumably because our reference DNA, which was bound to beads with both ends (beb), did not serve well as an undamaged control. Although Ku and RPA complexes were found enriched at beb DNA in comparison to oeb DNA, beb DNA-beads nevertheless triggered efficient γH2A.V phosphorylation, suggesting that the DNA ends were still somehow accessible. Alternatively, the incorporation of biotinylated nucleotides may have been recognized as a bulky DNA adduct. Indeed, we found that the incorporation of biotinylated nucleotides by nick translation triggers γH2A.V phosphorylation (data not shown). We also attempted to purify soluble linear and circular chromatin by various means to circumvent end-biotinylation, but the degree of purity achieved was not satisfactory due to the very high extract protein concentrations. Of note, the phosphoproteome analysis did not suffer from this limitation, since we compared soluble, not immobilized DNA.

We found the sensors of both alternative repair pathways, NHEJ (Ku70/Ku80 complex, Lig4) and HR (MRN and RPA complexes), conceivably because our extract is derived from asynchronous embryos and thus contains active components of all cell cycle stages. Ku associated with free DNA ends within minutes of incubation in the extract and remained bound, although delocalized. By contrast, DNA resection and RPA binding were only observed with delay. The fact that Ku70 was found to be phosphorylated at a residue implicated in lowering its affinity for DNA suggests that Ku dissociation from some ends relieved the inhibition of exonuclease leading to loss of DNA upon extended incubation (66).

Other known DNA damage-associated proteins were not found in reconstituted chromatin, such as the MDC1 ortholog Mu2, Xrcc4, Lig3, Xlf, Exo1, Dna2 and Xrcc1, even though these proteins exist in *Drosophila*. The lack of detection may be explained by technical limitations or may reflect the specific properties of the syncytial embryos system. Several proteins were not detected on reconstituted chromatin,

but phosphopeptides derived from them were observed in our phosphoproteome analysis, in a DNA- or even break-dependent manner (e.g. Mu2, Xrcc1, Lig3), reflecting the increased sensitivity of the latter due to phosphopeptide enrichment. Further proteins that could not be detected may only associate weakly or transiently with chromatin. Future improvements in mass spectrometry technology will allow a more comprehensive description of the system. However, there may also be physiological reasons why repair proteins are not present on damaged DNA. This raises the question of the nature of the DNA damage response in our system. Preblastoderm embryos are characterized by rapid nuclear divisions: the first 14 'cleavage state' divisions happen in ∼1.5 h, with shortened cell cycles lacking the gap phases (19,67), leaving no time for HR repair. In these early phases, the classical DNA replication/damage checkpoint is not active; ATM and Chk1 are present but exert their function only at cycle14 (21). At the same time, the checkpoint kinase dmChk2 senses genotoxic damage and triggers the elimination of fatally damaged nuclei in what has been called the 'mitotic catastrophe' (20,68). In case of damage, Chk2 localizes to the centrosomes, where it triggers centrosome instability and disruption of the mitotic spindle. The disconnection of nuclei to cortical centrosomes leads to the 'dropping out' of nuclei into the central yolk of the embryo, where they are degraded (20). Interestingly, injection of linear DNA fragments into cleavage stage embryos leads to centrosome defects, indicating a mechanism to prevent segregation of damaged chromosomes to maintain genomic stability (20). Key targets for Chk2 may reside in the γ-tubulin complex that initiates microtubule polymerization or in dynein/dynein-binding proteins. It will be interesting to explore whether the phosphorylation of the kinetochore proteins and microtubule-associated proteins, we observe in the presence of free DNA ends, are part of the physiological damage response.

γH2A.V signalling and spreading

Preblastoderm embryos do not normally mount a DNA damage response involving large domains of γH2A.V, because they do not engage in time-consuming repair by homologous recombination. However, evidently all components of this DSB signalling are present and active in the cell-free system. The efficiency of the reaction provides us with a unique opportunity to study the spreading of the phospho-mark. The γH2A.V signal appeared within a few minutes after incubation in our extract and remained on chromatin within the investigated time frames of up to 6 h, conceivably, because no significant repair was accomplished (14,69,70). The most remarkable observation in our study is the rapid spreading of the γH2A.V signal along the broken chromatin fragment over long distances without transfer onto undamaged DNA in the same cell-free reaction.

Spreading of the γH2A.X signal from a chromosomal break over long distances is a conserved feature of the DNA damage response: in yeast spreading of the mark has been observed for up to 300 kb and in mammals for even up to 2 MB (22,23,71). However, the mechanism of γH2A.X/H2A.V spreading is only poorly understood. Therefore, we applied our *in vitro* system and found that, after a short lag phase, the phosphorylation spreads very fast from the free DNA end to cover the entire molecule. Since it was difficult to trap intermediate stages with clear gradients of phosphorylation originating from the break site, our findings are consistent with a model according to which the modification propagates through transient contacts of nucleosomes in 'clutches' or 'crumbles' in the folded fibre for short ranges (72) and by dynamic loop formation of chromatin segments over slightly larger distances (73).

Reconstituting complex chromatin structures in a cell-free system

Key to a mechanistic understanding of the processes revolving around damaged chromatin is the development of cell-free systems that recapitulate specific aspects of the physiological chromatin damage response. Only a few *in vitro* systems are able to reconstitute complex chromatin with physiological nucleosome spacing [reviewed in (74,75)]. The most widely used system for assembly of dynamic chromatin that responds to DNA damage is derived from *Xenopus* eggs, where repair of pyrimidine dimers, interstrand crosslinks, topoisomerase II adducts and O6-methylguanine have been studied (6,76–78). *Xenopus* egg extracts have also been used very successfully to study the loading and unloading of proteins to DSBs (21,79–82), NHEJ (83), the replication at DSBs (84) and DSB repair during mitosis (85). A strength of the *Xenopus* system is that the extracts can be arrested to perform cell-cycle studies.

Here, we introduce a complementary *in vitro* system for mechanistic dissection of the DNA damage response in the *Drosophila* model system. Preblastoderm embryos contain all components required to support the first 14 rapid nuclei divisions, including chromatin assembly and DNA damage signalling (67,86,87). Preblastoderm embryo extracts allow the efficient assembly of complex chromatin with unique dynamic properties (27,88), which enabled the pioneering discovery of ATP-dependent nucleosome sliding factors (10–12) and fundamental properties of chromatin organization (13).

An advantage of the described system is its efficiency and reproducibility of preparing active extracts (89). *Drosophila*, being one of the major systems to study fundamental metazoan biology, is readily tractable by genetic approaches and supported by a wide range of available reagents, such as cell lines and antibodies. This greatly facilitates *in vivo* validation and follow-up studies of any phenomenon identified in the cell-free system. Researchers will welcome the cell-free system as new tool to complement their genetic and cell biological studies to study the specific DNA damage response that lead to the 'mitotic catastrophe' in syncytial embryos, However, a general limitation of cell-free systems is the absence of nuclear membranes and the spatial organization of the nucleus. A specific drawback of the *Drosophila* system is the lack of cell cycle synchrony in extracts and therefore the inability to study replication-associated processes.

Beyond these *Drosophila*-specific applications, we anticipate that the system will be useful to explore general, conserved aspects of the DSB response, such as the spreading of the γH2A.X along chromatin to create damage response domains, the recognition of DNA ends by dedicated sen-

sor complexes, the role of nucleosome remodelling factors in DNA resection and the regulated assembly of telomere capping complexes.

DATA AVAILABILITY

Next-generation sequencing data are uploaded to the GEO repository under the identifier GSE126415.

Proteome and phosphoproteome data can be accessed via Proteome Xchange/Pride under the identifiers PXD012990 and PXD013130, respectively.

SUPPLEMENTARY DATA

Supplementary Data are available at NAR Online.

ACKNOWLEDGEMENTS

We thank Stefan Krebs and the LAFUGA Genomics Facility for next-generation sequencing, Angelika Zabel for the preparation of sequencing libraries, Catherine Regnard for histones, Jürg Müller, Boris Pfander, Shelby Blythe, Moritz Völker-Albert and Alexander Konev for helpful discussions.

FUNDING

Deutsche Forschungsgemeinschaft [SFB 1064-A01 to P.B.B.; SFB 1321; INST 86/1800-1 FUGG to M.S.R.]; Swiss National Science Foundation [Advanced Postdoc Mobility Fellowship to S.B.]. The open access publication charge for this paper has been waived by Oxford University Press – *NAR* Editorial Board members are entitled to one free paper per year in recognition of their work on behalf of the journal.

Conflict of interest statement. None declared.

REFERENCES

1. Polo,S.E. and Almouzni,G. (2015) Chromatin dynamics after DNA damage: The legacy of the access-repair-restore model. *DNA Repair*, **36**, 114–121.
2. Dantuma,N.P. and van Attikum,H. (2016) Spatiotemporal regulation of posttranslational modifications in the DNA damage response. *EMBO J.*, **35**, 6–23.
3. Aleksandrov,R., Dotchev,A., Poser,I., Krastev,D., Georgiev,G., Panova,G., Babukov,Y., Danovski,G., Dyankova,T., Hubatsch,L. *et al.* (2018) Protein dynamics in complex DNA lesions. *Mol. Cell*, **69**, 1046–1061.
4. Hauer,M.H. and Gasser,S.M. (2017) Chromatin and nucleosome dynamics in DNA damage and repair. *Genes Dev.*, **31**, 2204–2221.
5. Soria,G., Polo,S.E. and Almouzni,G. (2012) Prime, repair, restore: the active role of chromatin in the DNA damage response. *Mol. Cell*, **46**, 722–734.
6. Sannino,V., Pezzimenti,F., Bertora,S. and Costanzo,V. (2017) Xenopus laevis as model system to study DNA damage response and replication fork stability. *Meth. Enzymol.*, **591**, 211–232.
7. Becker,P.B. and Wu,C. (1992) Cell-free system for assembly of transcriptionally repressed chromatin from Drosophila embryos. *Mol. Cell Biol.*, **12**, 2241–2249.
8. Becker,P.B., Tsukiyama,T. and Wu,C. (1994) Chromatin assembly extracts from Drosophila embryos. *Methods Cell Biol.*, **44**, 207–223.
9. Edgar,B.A. and O'Farrell,P.H. (1989) Genetic control of cell division patterns in the Drosophila embryo. *Cell*, **57**, 177–187.
10. Tsukiyama,T. and Wu,C. (1995) Purification and properties of an ATP-dependent nucleosome remodeling factor. *Cell*, **83**, 1011–1020.
11. Varga-Weisz,P.D., Wilm,M., Bonte,E., Dumas,K., Mann,M. and Becker,P.B. (1997) Chromatin-remodelling factorCHRAC contains the ATPasesISWI and topoisomerase II. *Nature*, **388**, 598–602.
12. Ito,T., Bulger,M., Pazin,M.J., Kobayashi,R. and Kadonaga,J.T. (1997) ACF, an ISWI-containing and ATP-utilizing chromatin assembly and remodeling factor. *Cell*, **90**, 145–155.
13. Baldi,S., Jain,D.S., Harpprecht,L., Zabel,A., Scheibe,M., Butter,F., Straub,T. and Becker,P.B. (2018) Genome-wide rules of nucleosome phasing in Drosophila. *Mol. Cell*, **72**, 661–672.
14. Kinner,A., Wu,W., Staudt,C. and Iliakis,G. (2008) Gamma-H2AX in recognition and signaling of DNA double-strand breaks in the context of chromatin. *Nucleic Acids Res.*, **36**, 5678–5694.
15. Talbert,P.B. and Henikoff,S. (2010) Histone variants–ancient wrap artists of the epigenome. *Nat. Rev. Mol. Cell Biol.*, **11**, 264–275.
16. Baldi,S. and Becker,P.B. (2013) The variant histone H2A.V of Drosophila—three roles, two guises. *Chromosoma*, **122**, 245–258.
17. Hong,S.-T. and Choi,K.-W. (2013) TCTP directly regulates ATM activity to control genome stability and organ development in Drosophila melanogaster. *Nat. Commun.*, **4**, 1–14.
18. Joyce,E.F., Pedersen,M., Tiong,S., White-Brown,S.K., Paul,A., Campbell,S.D. and McKim,K.S. (2011) Drosophila ATM and ATR have distinct activities in the regulation of meiotic DNA damage and repair. *J. Cell Biol.*, **195**, 359–367.
19. Yuan,K., Seller,C.A., Shermoen,A.W. and O'Farrell,P.H. (2016) Timing the Drosophila Mid-Blastula Transition: A cell Cycle-Centered view. *Trends Genet.*, **32**, 496–507.
20. Takada,S., Kelkar,A. and Theurkauf,W.E. (2003) Drosophila checkpoint kinase 2 couples centrosome function and spindle assembly to genomic integrity. *Cell*, **113**, 87–99.
21. Sibon,O.C., Laurençon,A., Hawley,R. and Theurkauf,W.E. (1999) The Drosophila ATM homologue Mei-41 has an essential checkpoint function at the midblastula transition. *Curr. Biol.*, **9**, 302–312.
22. Lee,C.-S., Lee,K., Legube,G. and Haber,J.E. (2014) Dynamics of yeast histone H2A and H2B phosphorylation in response to a double-strand break. *Nat. Struct. Mol. Biol.*, **21**, 103–109.
23. Iacovoni,J.S., Caron,P., Lassadi,I., Nicolas,E., Massip,L., Trouche,D. and Legube,G. (2010) High-resolution profiling of γH2AX around DNA double strand breaks in the mammalian genome. *EMBO J.*, **29**, 1446–1457.
24. Ejsmont,R.K., Sarov,M., Winkler,S., Lipinski,K.A. and Tomancak,P. (2009) A toolkit for high-throughput, cross-species gene engineering in Drosophila. *Nat. Methods*, **6**, 435–437.
25. Sandaltzopoulos,R. and Becker,P.B. (1994) Solid phase DNase I footprinting: quick and versatile. *Nucleic Acids Res.*, **22**, 1511–1512.
26. Postow,L., Ghenoiu,C., Woo,E.M., Krutchinsky,A.N., Chait,B.T. and Funabiki,H. (2008) Ku80 removal from DNA through double strand break-induced ubiquitylation. *J. Cell Biol.*, **182**, 467–479.
27. Völker-Albert,M.C., Pusch,M.C., Fedisch,A., Schilcher,P., Schmidt,A. and Imhof,A. (2016) A quantitative proteomic analysis of in vitro assembled chromatin. *Mol. Cell Proteom.*, **15**, 945–959.
28. Humphrey,S.J., Karayel,O., James,D.E. and Mann,M. (2018) High-throughput and high-sensitivity phosphoproteomics with the EasyPhos platform. *Nat. Protoc.*, **13**, 1897–1916.
29. Tyanova,S., Temu,T. and Cox,J. (2016) The MaxQuant computational platform for mass spectrometry-based shotgun proteomics. *Nat. Protoc.*, **11**, 2301–2319.
30. Klinker,H., Haas,C., Harrer,N., Becker,P.B. and Mueller-Planitz,F. (2014) Rapid purification of recombinant histones. *PLoS ONE*, **9**, e104029.
31. Li,Z., Johnson,M.R., Ke,Z., Chen,L. and Welte,M.A. (2014) Drosophila lipid droplets buffer the H2Av supply to protect early embryonic development. *Curr. Biol.*, **24**, 1485–1491.
32. Sandaltzopoulos,R., Blank,T.A. and Becker,P.B. (1994) Transcriptional repression by nucleosomes but not H1 in reconstituted preblastoderm Drosophila chromatin. *EMBO J.*, **13**, 373–379.
33. Paull,T.T., Rogakou,E.P., Yamazaki,V., Kirchgessner,C.U., Gellert,M. and Bonner,W.M. (2000) A critical role for histone H2AX in recruitment of repair factors to nuclear foci after DNA damage. *Curr. Biol.*, **10**, 886–895.
34. Anger,A.M., Armache,J.-P., Berninghausen,O., Habeck,M., Subklewe,M., Wilson,D.N. and Beckmann,R. (2013) Structures of the human and Drosophila 80S ribosome. *Nature*, **497**, 80–85.

35. Gebauer,F., Corona,D.F., Preiss,T., Becker,P.B. and Hentze,M.W. (1999) Translational control of dosage compensation in Drosophila by Sex-lethal: cooperative silencing via the 5′ and 3′ UTRs of msl-2 mRNA is independent of the poly(A) tail. *EMBO J.*, **18**, 6146–6154.
36. Liptak,C. and Loria,J.P. (2015) Movement and specificity in a modular DNA binding protein. *Struct./Fold. Design*, **23**, 973–974.
37. Sander,M., Lowenhaupt,K. and Rich,A. (1991) Drosophila Rrp1 protein: an apurinic endonuclease with homologous recombination activities. *Proc. Natl. Acad. Sci. U.S.A.*, **88**, 6780–6784.
38. Sander,M. and Benhaim,D. (1996) Drosophila Rrp1 3′-exonuclease: demonstration of DNA sequence dependence and DNA strand specificity. *Nucleic Acids Res.*, **24**, 3926–3933.
39. Pérez-Montero,S., Carbonell,A., Morán,T., Vaquero,A. and Azorín,F. (2013) The embryonic linker histone H1 variant of Drosophila, dBigH1, regulates zygotic genome activation. *Development. Cell*, **26**, 578–590.
40. Brodsky,M.H., Weinert,B.T., Tsang,G., Rong,Y.S., McGinnis,N.M., Golic,K.G., Rio,D.C. and Rubin,G.M. (2004) Drosophila melanogaster MNK/Chk2 and p53 regulate multiple DNA repair and apoptotic pathways following DNA damage. *Mol. Cell Biol.*, **24**, 1219–1231.
41. Sekelsky,J. (2017) DNA repair in Drosophila: Mutagens, models, and missing genes. *Genetics*, **205**, 471–490.
42. Mimori,T. and Hardin,J.A. (1986) Mechanism of interaction between Ku protein and DNA. *J. Biol. Chem.*, **261**, 10375–10379.
43. Yang,G., Liu,C., Chen,S.-H., Kassab,M.A., Hoff,J.D., Walter,N.G. and Yu,X. (2018) Super-resolution imaging identifies PARP1 and the Ku complex acting as DNA double-strand break sensors. *Nucleic Acids Res.*, **46**, 3446–3457.
44. Larcher,M.V., Pasquier,E., MacDonald,R.S. and Wellinger,R.J. (2016) Ku binding on telomeres occurs at sites distal from the physical chromosome ends. *PLoS Genet.*, **12**, e1006479-29.
45. Yuan,Y., Britton,S., Delteil,C., Coates,J., Jackson,S.P., Barboule,N., Frit,P. and Calsou,P. (2015) Single-stranded DNA oligomers stimulate error-prone alternative repair of DNA double-strand breaks through hijacking Ku protein. *Nucleic Acids Res.*, **43**, 10264–10276.
46. Attikum,H.V. and Gasser,S.M. (2014) ATP-Dependent chromatin remodeling and DNA Double-Strand break repair. *Cell Cycle*, **4**, 1011–1014.
47. Goldstein,M., Derheimer,F.A., Tait-Mulder,J. and Kastan,M.B. (2013) Nucleolin mediates nucleosome disruption critical for DNA double-strand break repair. *Proc. Natl. Acad. Sci. U.S.A.*, **110**, 16874–16879.
48. Maier,V.K., Chioda,M., Rhodes,D. and Becker,P.B. (2007) ACF catalyses chromatosome movements in chromatin fibres. *EMBO J.*, **27**, 817–826.
49. Corona,D.F., Eberharter,A., Budde,A., Deuring,R., Ferrari,S., Varga-Weisz,P., Wilm,M., Tamkun,J. and Becker,P.B. (2000) Two histone fold proteins, CHRAC-14 and CHRAC-16, are developmentally regulated subunits of chromatin accessibility complex (CHRAC). *EMBO J.*, **19**, 3049–3059.
50. Mathew,V., Pauleau,A.-L., Steffen,N., Bergner,A., Becker,P.B. and Erhardt,S. (2014) The histone-fold protein CHRAC14 influences chromatin composition in response to DNA damage. *Cell Rep.*, **7**, 321–330.
51. Lan,L., Ui,A., Nakajima,S., Hatakeyama,K., Hoshi,M., Watanabe,R., Janicki,S.M., Ogiwara,H., Kohno,T., Kanno,S.-I. *et al.* (2010) The ACF1 complex is required for DNA double-strand break repair in human cells. *Mol. Cell*, **40**, 976–987.
52. Lee,K.-J., Saha,J., Sun,J., Fattah,K.R., Wang,S.-C., Jakob,B., Chi,L., Wang,S.-Y., Taucher-Scholz,G., Davis,A.J. *et al.* (2016) Phosphorylation of Ku dictates DNA double-strand break (DSB) repair pathway choice in S phase. *Nucleic Acids Res.*, **44**, 1732–1745.
53. Byrne,B.M. and Oakley,G.G. (2019) Replication protein A, the laxative that keeps DNA regular: The importance of RPA phosphorylation in maintaining genome stability. *Semin. Cell Dev. Biol.*, **86**, 112–120.
54. Zhang,Y., Zhang,L., Tang,X., Bhardwaj,S.R., Ji,J. and Rong,Y.S. (2016) MTV, an ssDNA Protecting Complex Essential for Transposon-Based Telomere Maintenance in Drosophila. *PLoS Genet.*, **12**, e1006435.
55. Cenci,G., Siriaco,G., Raffa,G.D., Kellum,R. and Gatti,M. (2003) The Drosophila HOAP protein is required for telomere capping. *Nat. Cell Biol.*, **5**, 82–84.
56. Gao,G., Bi,X., Chen,J., Srikanta,D. and Rong,Y.S. (2009) Mre11-Rad50-Nbs complex is required to cap telomeres during Drosophila embryogenesis. *Proc. Natl. Acad. Sci. U.S.A.*, **106**, 10728–10733.
57. Ciapponi,L., Cenci,G., Ducau,J., Flores,C., Johnson-Schlitz,D., Gorski,M.M., Engels,W.R. and Gatti,M. (2004) The Drosophila Mre11/Rad50 complex is required to prevent both telomeric fusion and chromosome breakage. *Curr. Biol.*, **14**, 1360–1366.
58. Musarò,M., Ciapponi,L., Fasulo,B., Gatti,M. and Cenci,G. (2008) Unprotected Drosophila melanogaster telomeres activate the spindle assembly checkpoint. *Nat. Genet.*, **40**, 362–366.
59. Williams,B.C., Li,Z., Liu,S., Williams,E.V., Leung,G., Yen,T.J. and Goldberg,M.L. (2003) Zwilch, a new component of the ZW10/ROD complex required for kinetochore functions. *Mol. Biol. Cell*, **14**, 1379–1391.
60. Kachaner,D., Pinson,X., El Kadhi,K.B., Normandin,K., Talje,L., Lavoie,H., Lépine,G., Carréno,S., Kwok,B.H., Hickson,G.R. *et al.* (2014) Interdomain allosteric regulation of Polo kinase by Aurora B and Map205 is required for cytokinesis. *J. Cell Biol.*, **207**, 201–211.
61. Tan,S., Lyulcheva,E., Dean,J. and Bennett,D. (2008) Mars promotes dTACC dephosphorylation on mitotic spindles to ensure spindle stability. *J. Cell Biol.*, **182**, 27–33.
62. Ravi,D., Wiles,A.M., Bhavani,S., Ruan,J., Leder,P. and Bishop,A.J.R. (2009) A network of conserved damage survival pathways revealed by a genomic RNAi screen. *PLoS Genet.*, **5**, e1000527.
63. Chang,H.H.Y., Pannunzio,N.R., Adachi,N. and Lieber,M.R. (2017) Non-homologous DNA end joining and alternative pathways to double-strand break repair. *Nat. Rev. Mol. Cell Biol.*, **18**, 495–506.
64. Symington,L.S. and Gautier,J. (2011) Double-strand break end resection and repair pathway choice. *Annu. Rev. Genet.*, **45**, 247–271.
65. Mitsis,P.G., Kowalczykowski,S.C. and Lehman,I.R. (1993) A single-stranded DNA binding protein from Drosophila melanogaster: characterization of the heterotrimeric protein and its interaction with single-stranded DNA. *Biochemistry*, **32**, 5257–5266.
66. Clerici,M., Mantiero,D., Guerini,I., Lucchini,G. and Longhese,M.P. (2008) The Yku70–Yku80 complex contributes to regulate double-strand break processing and checkpoint activation during the cell cycle. *EMBO Rep.*, **9**, 810–818.
67. Farrell,J.A. and O'Farrell,P.H. (2014) From egg to gastrula: how the cell cycle is remodeled during the Drosophila mid-blastula transition. *Annu. Rev. Genet.*, **48**, 269–294.
68. Iampietro,C., Bergalet,J., Wang,X., Cody,N.A.L., Chin,A., Lefebvre,F.A., Douziech,M., Krause,H.M. and Lécuyer,E. (2014) Developmentally regulated elimination of damaged nuclei involves a Chk2-dependent mechanism of mRNA nuclear retention. *Development. Cell*, **29**, 468–481.
69. Chowdhury,D., Keogh,M.-C., Ishii,H., Peterson,C.L., Buratowski,S. and Lieberman,J. (2005) gamma-H2AX dephosphorylation by protein phosphatase 2A facilitates DNA double-strand break repair. *Mol. Cell*, **20**, 801–809.
70. Moon,S.-H., Nguyen,T.-A., Darlington,Y., Lu,X. and Donehower,L.A. (2014) Dephosphorylation of γ-H2AX by WIP1: An important homeostatic regulatory event in DNA repair and cell cycle control. *Cell Cycle*, **9**, 2092–2096.
71. Shroff,R., Arbel-Eden,A., Pilch,D., Ira,G., Bonner,W.M., Petrini,J.H., Haber,J.E. and Lichten,M. (2004) Distribution and dynamics of chromatin modification induced by a defined DNA double-strand break. *Curr. Biol.*, **14**, 1703–1711.
72. Ricci,M.A., Manzo,C., García-Parajo,M.F., Lakadamyali,M. and Cosma,M.P. (2015) Chromatin fibers are formed by heterogeneous groups of nucleosomes in vivo. *Cell*, **160**, 1145–1158.
73. Erdel,F. and Greene,E.C. (2016) Generalized nucleation and looping model for epigenetic memory of histone modifications. *Proc. Natl. Acad. Sci. U.S.A.*, **113**, E4180–E4189.
74. Liu,X. (2015) In vitro chromatin templates to study nucleotide excision repair. *DNA Repair*, **36**, 68–76.
75. Garner,E. and Costanzo,V. (2009) Studying the DNA damage response using in vitro model systems. *DNA Repair*, **8**, 1025–1037.
76. Gaillard,P.H., Martini,E.M., Kaufman,P.D., Stillman,B., Moustacchi,E. and Almouzni,G. (1996) Chromatin assembly coupled to DNA repair: a new role for chromatin assembly factor I. *Cell*, **86**, 887–896.

77. Aparicio,T., Baer,R., Gottesman,M. and Gautier,J. (2016) MRN, CtIP, and BRCA1 mediate repair of topoisomerase II-DNA adducts. *J. Cell Biol.*, **212**, 399–408.
78. Olivera Harris,M., Kallenberger,L., Artola Borán,M., Enoiu,M., Costanzo,V. and Jiricny,J. (2015) Mismatch repair-dependent metabolism of O6-methylguanine-containing DNA in Xenopus laevis egg extracts. *DNA Repair*, **28**, 1–7.
79. Postow,L., Woo,E.M., Chait,B.T. and Funabiki,H. (2009) Identification of SMARCAL1 as a component of the DNA damage response. *J. Biol. Chem.*, **284**, 35951–35961.
80. Schrank,B.R., Aparicio,T., Li,Y., Chang,W., Chait,B.T., Gundersen,G.G., Gottesman,M.E. and Gautier,J. (2018) Nuclear ARP2/3 drives DNA break clustering for homology-directed repair. *Nature*, **559**, 61–66.
81. Di Virgilio,M., Ying,C.Y. and Gautier,J. (2009) PIKK-dependent phosphorylation of Mre11 induces MRN complex inactivation by disassembly from chromatin. *DNA Repair*, **8**, 1311–1320.
82. Liao,S., Guay,C., Toczylowski,T. and Yan,H. (2012) Analysis of MRE11's function in the 5′→3′ processing of DNA double-strand breaks. *Nucleic Acids Res.*, **40**, 4496–4506.
83. Graham,T.G.W., Walter,J.C. and Loparo,J.J. (2017) Ensemble and Single-Molecule analysis of Non-Homologous end joining in frog egg extracts. *Meth. Enzymol.*, **591**, 233–270.
84. Wawrousek,K.E., Fortini,B.K., Polaczek,P., Chen,L., Liu,Q., Dunphy,W.G. and Campbell,J.L. (2010) Xenopus DNA2 is a helicase/nuclease that is found in complexes with replication proteins And-1/Ctf4 and Mcm10 and DSB response proteins Nbs1 and ATM. *Cell Cycle*, **9**, 1156–1166.
85. Smith,E. and Costanzo,V. (2009) Responding to chromosomal breakage during M-phase: insights from a cell-free system. *Cell Div*, **4**, 15.
86. Blythe,S.A. and Wieschaus,E.F. (2015) Coordinating cell cycle remodeling with transcriptional activation at the Drosophila MBT. *Curr. Top. Dev. Biol.*, **113**, 113–148.
87. Langley,A.R., Smith,J.C., Stemple,D.L. and Harvey,S.A. (2014) New insights into the maternal to zygotic transition. *Development*, **141**, 3834–3841.
88. Varga-Weisz,P.D., Blank,T.A. and Becker,P.B. (1995) Energy-dependent chromatin accessibility and nucleosome mobility in a cell-free system. *EMBO J.*, **14**, 2209–2216.
89. Blank,T.A., Sandaltzopoulos,R. and Becker,P.B. (1997) Biochemical analysis of chromatin structure and function using Drosophila embryo extracts. *Methods*, **12**, 28–35.